

# Searching for single production of vector-like quarks decaying into $Wb$ at a future muon-proton collider

Jin-Zhong Han<sup>1\*</sup>, Yao-Bei Liu<sup>2†</sup>, and Stefano Moretti<sup>3,4‡</sup>

1. *School of Physics and Telecommunications Engineering,  
Zhoukou Normal University, Zhoukou 466001, P.R. China*

2. *Henan Institute of Science and Technology, Xinxiang 453003, P.R. China*

3. *School of Physics & Astronomy, University of Southampton,  
Highfield, Southampton SO17 1BJ, UK*

4. *Department of Physics & Astronomy,  
Uppsala University, Box 516, 751 20 Uppsala, Sweden*

## Abstract

In this work, we investigate the single production of the Vector-Like Quarks (VLQs)  $T$  and  $Y$ , with charge  $+2/3e$  and  $-4/3e$ , respectively, both decaying into  $Wb$  at a future  $\mu p$  collider with  $\sqrt{s} = 5.29, 6.48$ , and  $9.16$  TeV. We focus on two final states, where the  $W$  boson decays leptonically or hadronically (in the latter case, it is highly boosted, leading to a fat  $W$ -jet). By performing a detailed signal-to-background analysis in presence of detector simulations, the  $5\sigma$  discovery prospects and 95% CL exclusion limits are mapped over parameter space regions of the model accommodating such new heavy quarks, assuming an integrated luminosity of  $100 \text{ fb}^{-1}$  at each of the aforementioned energies.

---

\* E-mail: hanjinzhong@zknu.edu.cn

† E-mail: liuyaobei@hist.edu.cn

‡ E-mail: stefano.moretti@cern.ch

## I. INTRODUCTION

Vector-like quarks (VLQs) with masses at the TeV scale are generally predicted in a variety of extensions of the Standard Model (SM), such as the little Higgs models [1–4], composite Higgs models [5–8], two-Higgs-doublet models [9–14], and other extended models [15–18]. A common feature of these new particles is that the left- and right-handed chiral components transform in the same way under the Electro-Weak (EW) symmetry group of the SM [19]. Unlike for chiral quarks, bare mass terms of VLQs are gauge invariant and therefore they can avoid the strict constraints by the Higgs boson data<sup>1</sup>. Moreover, VLQs have the potential to stabilize the EW vacuum [22, 23], the so-called Cabibbo-Kobayashi-Maskawa (CKM) unitarity problem [24–28], and may also provide explanations for various experimental anomalies, such as the  $W$ -mass one [29–33]. There exists three types of multiple VLQs, including EW singlet ( $T, B$ ), doublets [ $(X, T), (T, B)$  or  $(B, Y)$ ], and triplets [ $(X, T, B)$  or  $(T, B, Y)$ ]. In the models embedding these, VLQs are expected to couple preferentially to third-generation quarks and can give rise to a rich variety of phenomena at the Large Hadron Collider (LHC) and future high-energy colliders (for example, see [34–66]).

The VLQ  $T$ -state (VLQ- $T$ , also denoted  $T$  in the remainder) has an electric charge of  $+2/3e$  and occurs in any weak-isospin multiplet, whereas the VLQ  $Y$ -state (VLQ- $Y$ , also denoted by  $Y$  in the remainder), which has an electric charge of  $-(4/3)e$ , only appears in doublet or triplet representations. The singlet VLQ- $T$  has three possible decay modes:  $T \rightarrow bW, tZ$ , and  $th$  (unless an extended Higgs sector is present [48, 51]). In the high-mass limit, the Branching Ratios (BRs) are  $\text{BR}(T \rightarrow th) \approx \text{BR}(T \rightarrow tZ) \approx \frac{1}{2}\text{BR}(T \rightarrow Wb)$ . Due to its charge, the VLQ- $Y$  can decay only into  $Wb$  pairs with same charge with a BR of 100%. Up to now, the ATLAS and CMS Collaborations have conducted extensive VLQ searches for the (QCD induced) pair-production processes and the constraints on their masses have been obtained at a 95% Confidence Level (CL) [67–78]. For instance, the minimum mass of a singlet VLQ- $T$  ( $Y$ ) is set at about 1.36 (1.7) TeV from direct searches by the ATLAS Collaboration with an integrated luminosity of  $140 \text{ fb}^{-1}$  [67]. The CMS Collaboration have excluded a singlet (doublet) VLQ- $T$  mass below 1.46 (1.48) TeV at 95% C.L. by using  $138 \text{ fb}^{-1}$  of  $pp$  collision data in the leptonic

---

<sup>1</sup> An extra fourth generation of SM-like quarks [20, 21] should be much heavier due to the EW precision constraints.

final states [69]. In addition, such VLQ- $T$  can be singly produced at the LHC via EW interactions and the corresponding processes are highly sensitive to the couplings between VLQs and SM quarks [79–81]. Searches performed recently by the ATLAS and CMS Collaborations set limits on VLQs masses and couplings using Run 2 recorded data [82–89]. For a benchmark signal prediction of a  $SU(2)_L$  singlet VLQ- $T$  with the mixing parameter  $\kappa = 0.5$ , which governs VLQ interactions with SM particles, masses below 2.1 TeV are excluded by ATLAS with an integrated luminosity of  $139 \text{ fb}^{-1}$  [85]. For the VLQ- $Y$ , the strongest exclusion limit is set by ATLAS in the  $bbbq'$  final state, where  $\kappa \geq 0.3$  is excluded for mass near 2 TeV [86].

In this work, we consider a muon-proton collider with multi-TeV beam energies, which was proposed two decades ago [90–94], and more recently in Refs. [95–100]. Compared to a  $ep$  collider, a  $\mu p$  one can achieve a much higher center-of-mass energy and thus exotic particles production is more probable due to much larger scattering cross sections. Further, Beyond the SM (BSM) studies at these types of machines usually suffer from smaller QCD backgrounds than at  $pp$  colliders. Recently, a lot of related phenomenological work has been carried out for a future  $\mu p$  collider [101–110]. Phenomenological studies of VLQs at an  $ep$  colliders can be found in Refs. [111–115]. In this study, we will focus on the observability of single  $T/Y$  production at a future  $\mu p$  collider via the  $T/Y \rightarrow Wb$  decay channel both in the semileptonic and hadronic final states.

The paper is arranged as follows. In Sec. II, we consider a simplified model including the VLQ- $T/Y$  and present the cross sections for the single production process at a  $\mu p$  collider with three different center-of-mass energies. In Sec. III, we discuss its observability via the decay modes  $T/Y \rightarrow bW \rightarrow b\ell + \cancel{E}_T$  and  $T/Y \rightarrow bW \rightarrow bj j$ , where  $\ell$  is a lepton,  $\cancel{E}_T$  is the missing transverse energy, and  $j$  is a jet (notice that the two jets will merge into a single fat one  $J$ ). Finally, conclusions are presented in Sec. IV.

## II. THE SIMPLIFIED MODEL AND SINGLE $T/Y$ PRODUCTION AT A $\mu p$ COLLIDER

Following the notation of Ref. [35], a generic parametrization of an effective Lagrangian for a singlet VLQ- $T$  is given by

$$\mathcal{L}_T = \frac{gg^*}{2\sqrt{2}} [\bar{T}_L W_\mu^+ \gamma^\mu b_L + \frac{g}{\sqrt{2}c_W} \bar{T}_L Z_\mu \gamma^\mu t_L - \frac{m_T}{\sqrt{2}m_W} \bar{T}_R h t_L - \frac{m_t}{\sqrt{2}m_W} \bar{T}_L h t_R] + H.c., \quad (1)$$

where  $g$  is the  $SU(2)_L$  gauge coupling constant, and  $\theta_W$  is the Weinberg angle. Thus, there are only two model parameters: the VLQ- $T$  quark mass  $m_T$  and the coupling strength to SM quarks in units of standard couplings,  $g^*$ . As mentioned, the singlet VLQ- $T$  has three possible decay modes:  $T \rightarrow bW$ ,  $tZ$ , and  $th$ . For  $M_T \geq 1$  TeV, the BRs are  $\text{BR}(T \rightarrow th) \approx \text{BR}(T \rightarrow tZ) \approx \frac{1}{2}\text{BR}(T \rightarrow Wb)$ , which is a good approximation as expected from the Goldstone boson equivalence theorem [116–120].

Certainly, the coupling parameter,  $g^*$ , can also be described as other constants, i.e.,  $s_L$  in [19] and  $\kappa_T$  [35]. A simple relationship among these coupling parameters is:  $g^* = \sqrt{2}\kappa_T = 2s_L$  [121]. For  $m_T = 1.5$  (1.8) TeV,  $g^*$  should be smaller than about 0.42 (0.56) [121]. In this work we take only a phenomenologically guided limit:  $g^* \leq 0.5$ , in the region  $m_T \geq 1.5$  TeV.

Assuming that the VLQ- $Y$  only couples to the SM third generation quarks, an effective Lagrangian framework can be written as:

$$\mathcal{L}_Y = \frac{g\kappa_Y^{L/R}}{\sqrt{2}}[\bar{Y}_{L/R}W_\mu^- \gamma^\mu b_{L/R}] + H.c. \quad (2)$$

Note that we can assume  $\kappa_Y^L = 0$  for a  $(B, Y)$  doublet, and  $\kappa_Y^R = 0$  for a  $(T, B, Y)$  triplet [19]. The cross sections for the single production process and the kinematics of the final states studied here are similar for left-handed and right-handed couplings. For simplicity, we consider a benchmark scenario with right-handed couplings only in this work:  $\kappa_Y = \kappa_Y^R \neq 0$  and  $\kappa_Y^L = 0$ , as for example in the case of the  $(B, Y)$  doublet. For large mass values of the VLQ- $Y$ , the decay width is approximated as  $\Gamma_Y \sim \kappa_Y^2 m_Y^3 \times 3.28 \times 10^{-7} \text{ GeV}^{-2}$  [64].

From the above discussions, we know that the VLQ- $T/Y$  can be singly produced in  $\mu p$  collisions via  $Wb$  fusion process with a subsequent decay  $T/Y \rightarrow Wb$ . An example of a Leading Order (LO) Feynman diagram is depicted in Fig. 1.

The LO cross sections are obtained using MadGraph5-aMC@NLO [122] with default NNPDF23L01 Parton Distribution Functions (PDFs) [123] taking the default renormalization and factorization scales. The beam energies are taken to be  $E_p = 7$  TeV, and  $E_\mu = 1.0, 1.5$ , and 3 TeV, which correspond to three typical center-of-mass energies:

- $\mu p - 1$ :  $\sqrt{s} = 5.29$  TeV,
- $\mu p - 2$ :  $\sqrt{s} = 6.48$  TeV,
- $\mu p - 3$ :  $\sqrt{s} = 9.16$  TeV,

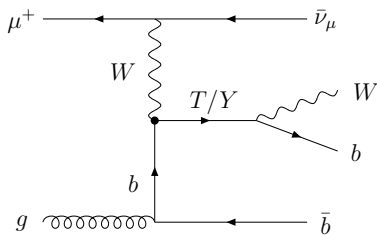


FIG. 1: Representative tree-level Feynman diagram for single production of VLQ- $T/Y$  at a  $\mu p$  collider followed by the  $T/Y \rightarrow bW$  decay channel.

respectively.

In Fig. 2, we show the dependence of the cross sections  $\sigma \times \text{BR}(T/Y \rightarrow bW)$  on the VLQ- $T/Y$  mass for  $g^*/\kappa_Y = 0.1$ . Note that the conjugate processes have also been included. As the VLQ mass grows, the cross section of single production decreases slowly due to a smaller phase space. For comparison, we also display the cross-sections for the single VLQ- $T$  production processes at the 14 TeV LHC,  $\sigma(pp \rightarrow Tb j) \times \text{BR}(T \rightarrow bW)$ , and the electron-hadron Future Circular Collider (FCC-eh),  $\sigma(ep \rightarrow \nu T j) \times \text{BR}(T \rightarrow bW)$  with  $\sqrt{s} = 3.46$  TeV, respectively. We also find that the cross sections can be up to about one order of magnitude larger than those at the FCC-eh, and even comparable to those at the LHC with  $\sqrt{s} = 14$  TeV. For  $g^*/\kappa_Y = 0.1$  and  $m_{T/Y} = 2$  TeV, the cross section can reach 0.4 (0.82), 1.3 (2.54) and 5.6 (11.4) fb, respectively, at a  $\mu p$  collider with three different center-of-mass energies. Certainly, the single production cross section is proportional to the square of the coupling strength  $g^*$  or  $\kappa_Y$ .

### III. COLLIDER SIMULATION AND ANALYSIS

Next we analyze the observation potential of the discussed  $\mu p$  processes by performing a Monte Carlo (MC) simulation of signals (and, eventually, also background) events generated by single VLQ- $T/Y$  production and the  $T/Y \rightarrow bW$  decay channel. Considering the case of the  $W$  boson decaying leptonically, the final events are required to have exactly one isolated identified lepton (specifically, an electron), at least one  $b$ -tagged jet and large missing transverse

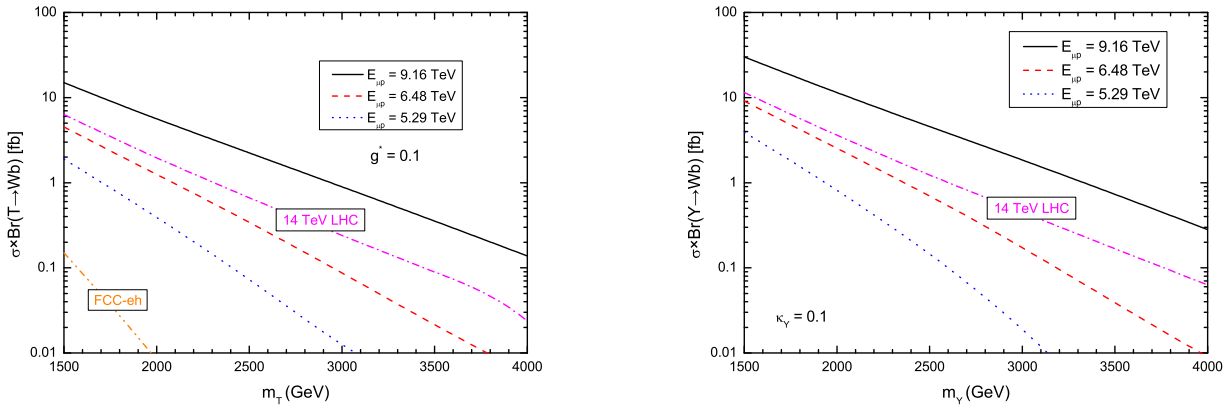


FIG. 2: Cross section of  $\sigma \times \text{BR}(T/Y \rightarrow bW)$  as a function of the VLQ mass for  $g^*/\kappa_Y = 0.1$  at a  $\mu p$  collider with three different center-of-mass energies. (The LHC and FCC-eh results for competing processes are also shown: see the text for details.)

energy from the escaping neutrino. (We do not consider the selection for the associated bottom quark from the splitting of an initial-stage gluon into a pair of  $b$ -quarks, which is often outside of the detector acceptance due to its typically low momentum.) To increase the signal rate, we also impose that the  $W$  boson decays into a pair of quarks where the emerging jets  $j$  can be collimated so as to appear as a fat jet ( $J$ ), for which a representative Feynman diagram is given in Fig. 3.

Note that the kinematics of the final states are similar for VLQ- $T$  and VLQ- $Y$ , so that the acceptances for the two types of VLQs are found to be the same. Thus, the VLQ- $Y$  signals were not simulated separately. Finally, since we are including charged conjugation and the charge of the jets is not reconstructed, the contributions to the signal of the  $T$  and  $Y$  mediated processes are indistinguishable so that, eventually, they can be summed over despite, in the remainder, they are considered separately (thus, by implicitly exploiting MC truth knowledge).

### A. Expected discovery and exclusion reach for VLQ- $T$

Next we perform a the signal-to-background analysis for the above two final states, which signal patterns are (to recap):

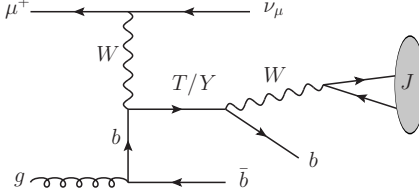


FIG. 3: Representative Feynman diagram for the  $b + J$  final state.

Case 1:  $\mu^+ p \rightarrow \bar{\nu}_\mu T(\rightarrow bW^+) \bar{b} \rightarrow \ell^+ b\bar{b} + \cancel{E}_T$  for  $W^+ \rightarrow \ell^+ \nu_\ell$  with  $\ell = e$ .

Case 2:  $\mu^+ p \rightarrow \bar{\nu}_\mu T(\rightarrow bW^+) \bar{b} \rightarrow J + b\bar{b} + \cancel{E}_T$  for  $W \rightarrow jj$  with  $j$  a light-quark jet.

Note that, for Case 1, we consider the final leptons to be only electrons due to large SM background processes  $\mu p \rightarrow \mu jj$  and  $\mu p \rightarrow \mu b\bar{b}$  whereas, for case 2, the two jets are tagged as a fat one  $J$  (as intimated). (In our simulation, the conjugate processes of all backgrounds have also been considered.) The dominant SM backgrounds for Case 1 come from the following processes:

- $\mu p \rightarrow \nu_\mu tb$  with  $t \rightarrow bW \rightarrow b\nu_e$ ;
- $\mu p \rightarrow \nu_\mu W j$  with  $W \rightarrow e\nu_e$ .

For Case 2, the dominant SM backgrounds come from the following processes:

- $\mu p \rightarrow \nu_\mu tb$  with  $t \rightarrow bW \rightarrow bjj$ ;
- $\mu p \rightarrow \nu_\mu W j$  with  $W \rightarrow jj$ ;
- $\mu p \rightarrow \nu_\mu Z j$  with  $Z \rightarrow q\bar{q}$  (where  $q$  is a quark from the first two generations) and  $Z \rightarrow b\bar{b}$ ;
- $\mu p \rightarrow \nu_\mu jj$ .

TABLE I: The cross sections of SM background for various experiments, in pb.

Process	decay channel	$\mu p - 1$	$\mu p - 2$	$\mu p - 3$
$\mu p \rightarrow \nu_\mu tb$	$t \rightarrow b\ell\nu$	12.8	17.6	29.7
	$t \rightarrow bjj$	38.2	52.9	89.1
$\mu p \rightarrow \nu_\mu W j$	$W \rightarrow \ell\nu$	3.7	4.76	7.16
	$W \rightarrow jj$	11.1	14.3	21.5
$\mu p \rightarrow \nu_\mu Z j$	$Z \rightarrow q\bar{q}, b\bar{b}$	5.37	6.98	10.7
$\mu p \rightarrow \nu_\mu jj$	\	378	480	701.4

Signal and background events are generated at LO using MadGraph5-aMC@NLO with the aforementioned PDFs. Further, parton showers and hadronization are performed using Pythia 8.3 [124]. Then, Delphes 3.4.2 [125] is used for fast detector simulation, using the standard LHeC detector card. In our analysis for the  $W$  fat jet, the jets are reconstructed by the Cambridge-Achen algorithm [126, 127], implemented in the FastJet package [128], assuming a cone radius  $R = 0.8$ . Finally, the reconstructed events are analysed using MadAnalysis 5 [129, 130].

To identify objects, the following basic (or generation) cuts are chosen:

$$p_T^{\ell/\text{jet}} > 15 \text{ GeV}, \quad |\eta_\ell| < 2.5, \quad |\eta_{\text{jet}}| < 5, \quad \Delta R_{xy} > 0.4, \quad (3)$$

where  $p_T^{\ell/\text{jet}}$  and  $|\eta_{\ell/\text{jet}}|$  are the transverse momentum and pseudorapidity of the electrons ( $\ell = e$ ) and jets  $b$  and  $J$ . Here,  $\Delta R(x, y) = \sqrt{\Delta\Phi^2 + \Delta\eta^2}$  is the separation in the pseudorapidity-azimuth plane between the pairs of objects  $x$  and  $y$ , where  $x, y = e, b, J$ , wherein  $b$  represents a  $b$ -tagged jet.

### 1. Analysis of signal events for Case 1

The following three signal benchmark points are taken with the fixed parameter  $g^* = 0.1$ :

- (i)  $T_{1500}$ :  $m_T = 1500 \text{ GeV}$ ;
- (ii)  $T_{2000}$ :  $m_T = 2000 \text{ GeV}$ ;

(iii)  $T_{2500}$ :  $m_T = 2500$  GeV.

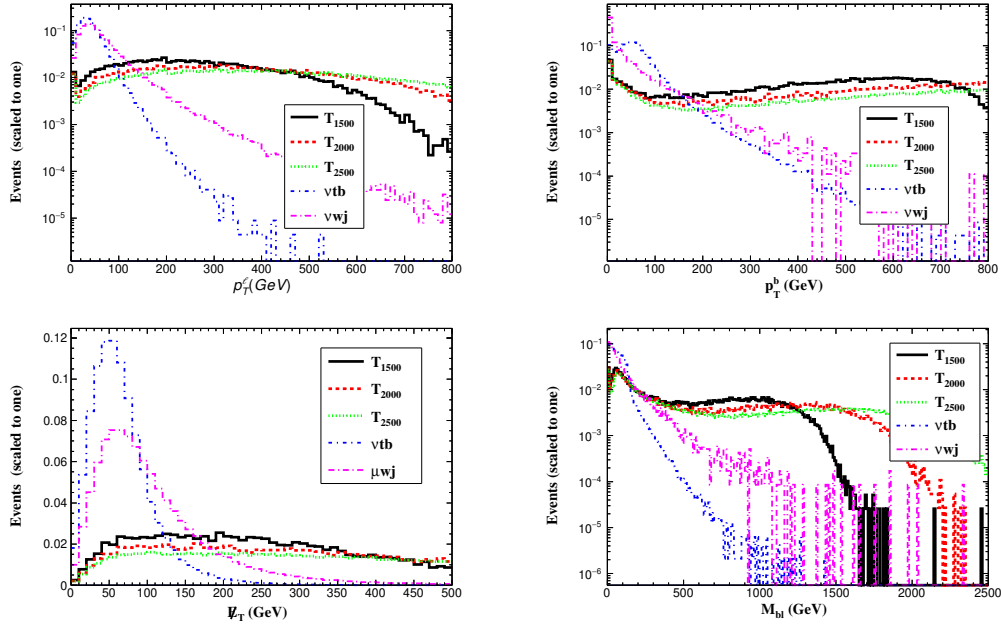


FIG. 4: Normalized distributions for the three signals (with  $m_T = 1500, 2000$ , and  $2500$  GeV) and SM backgrounds at  $\mu p - 1$ .

In Fig. 4, we plot some differential distributions for the three signal benchmark points ( $T_{1500}$ ,  $T_{2000}$  and  $T_{2500}$ ) and SM backgrounds for the  $\mu p - 1$  scenario, including the transverse momentum distributions of the lepton ( $p_T^e$ ) and the leading  $b$ -tagged jet ( $p_T^b$ ), the missing transverse energy  $\cancel{E}_T$  and the invariant mass distribution  $M_{be}$ . Because of the larger mass of VLQ- $T$ , the decay products are highly energetic, and thus the  $p_T^e$  and  $p_T^b$  peaks of the signals are larger than those of the SM backgrounds. According to the behaviors of these distributions, we impose the following cuts to distinguish the signal from the SM backgrounds.

- Cut 1: Exactly one isolated electron with  $p_T^e > 150$  GeV (i.e., events with final state muons or taus are vetoed).
- Cut 2: At least one  $b$ -tagged jet is required with  $p_T^b > 200$  GeV, and the pseudorapidity-azimuth distance between the  $b$ -tagged jet and the lepton is  $\Delta R_{e,b} > 2.7$ .
- Cut 3: The transverse missing energy is required to be  $\cancel{E}_T > 300$  GeV.

- Cut 4: The  $be$  invariant mass is required to be  $M_{be} > 1000$  GeV.

Since the behaviors of the relevant kinematic distributions at  $\mu p - 2$  and  $\mu p - 3$  are similar to the case of  $\mu p - 1$ , we do not display these here. Based on the behaviors of these distributions, we impose the same cuts to enhance the sensitivity also at  $\mu p - 2$  and  $\mu p - 3$ .

TABLE II: Cut flow of the cross sections (in fb) for the signals and SM backgrounds at  $\mu p - 1$  for the final state in Case 1. Here, we set a benchmark value of  $g^* = 0.1$ .

Cuts	Signals			Backgrounds	
	$T_{1500}$	$T_{2000}$	$T_{2500}$	$\nu tb$	$\nu W j$
Basic	0.35	0.074	0.014	7296	2331
Cut 1	0.12	0.028	0.0054	26	102
Cut 2	0.084	0.02	0.004	5.1	0.42
Cut 3	0.06	0.015	0.0032	0.84	0.13
Cut 4	0.024	0.012	0.003	0.077	0.037

TABLE III: Cut flow of the cross sections (in fb) for the signals and SM backgrounds at  $\mu p - 2$  for the final state in Case 1. Here, we set a benchmark value of  $g^* = 0.1$ .

Cuts	Signals			Backgrounds	
	$T_{1500}$	$T_{2000}$	$T_{2500}$	$\nu tb$	$\nu W j$
Basic	0.84	0.24	0.065	9328	2761
Cut 1	0.29	0.09	0.026	41	143
Cut 2	0.19	0.065	0.018	8.8	0.51
Cut 3	0.14	0.05	0.015	1.62	0.22
Cut 4	0.06	0.04	0.013	0.28	0.076

The cross sections of the three typical signals and the relevant SM backgrounds are presented in Tabs. II-IV after imposing the aforementioned cuts. Notably, all background processes are very significantly suppressed at the end of the cut flow, and the cross section of the total SM background is about 0.11 fb at  $\mu p - 1$ , 0.36 fb at  $\mu p - 2$  and 0.64 fb at  $\mu p - 3$ , respectively.

TABLE IV: Cut flow of the cross sections (in fb) for the signals and SM backgrounds at  $\mu p - 3$  for the final state in Case 1. Here, we set a benchmark value of  $g^* = 0.1$ .

Cuts	Signals			Backgrounds	
	$T_{1500}$	$T_{2000}$	$T_{2500}$	$\nu tb$	$\nu W j$
Basic	2.72	1.03	0.41	13055	3437
Cut 1	0.96	0.4	0.16	82	208
Cut 2	0.67	0.28	0.12	18	0.87
Cut 3	0.48	0.22	0.11	4.3	0.57
Cut 4	0.21	0.18	0.09	0.27	0.37

## 2. Analysis of signal events for Case 2

In Fig. 5, we show the normalized distributions of the transverse momentum of the fat jet ( $p_T^J$ ) and leading  $b$ -tagged jet ( $p_T^b$ ) as well as those of the the fat jet mass ( $M_J$ ) and of the invariant mass of the  $b$ -tagged and fat jet system ( $M_{b,J}$ ). (Again, these are presented for  $\mu p - 1$ , but they are very similar for  $\mu p - 2$  and  $\mu p - 3$ .) According to the behaviors of these distributions, we impose the following cuts to extract the signal from the SM backgrounds.

- Cut 1: The transverse momentum for the fat jet is required to be  $p_T^J > 200$  GeV.
- Cut 2: The fat jet mass is such that  $|M_J - m_W| < 15$  GeV.
- Cut 3: At least one  $b$ -tagged jet is required with  $p_T^b > 200$  GeV, and the pseudorapidity-azimuth distance between the  $b$ -tagged jet and the fat jet is  $\Delta R_{b,J} > 2.7$ .
- Cut 4: The aforementioned invariant mass is required to be:  $M_{b,J} > 1300$  GeV for  $m_T < 1800$  GeV (Cut 4a), and  $M_{b,J} > 1500$  GeV for  $m_T \geq 1800$  GeV (Cut 4b).

In Tabs. V-VII, we present the cross sections for the signals and relevant SM backgrounds after imposing the above cuts. Here, one can see that all the SM backgrounds are suppressed very efficiently, while the signals still have relatively good efficiency at the end of the cut flow. The cross section of the total SM background for Case 2 is about 0.28 fb at  $\mu p - 1$ , 0.52 fb at  $\mu p - 2$  and 1.65 fb at  $\mu p - 2$ , respectively.

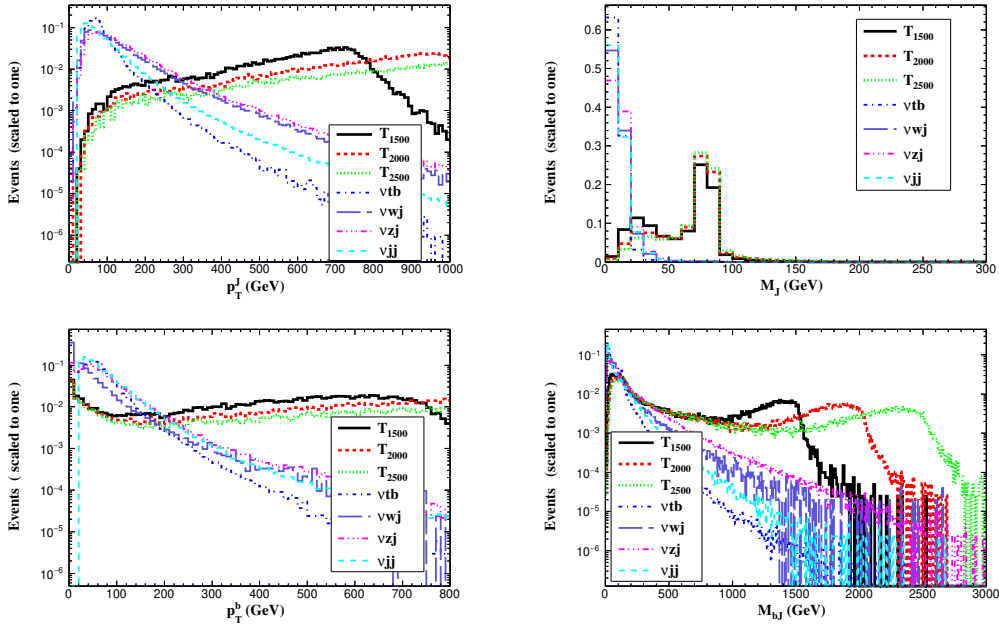


FIG. 5: Normalized distributions for the signals (with  $m_T = 1500, 2000$  and  $2500$  GeV) and SM backgrounds at  $\mu_{up} = 1$ .

### 3. Discovery and exclusion significance

In order to analyze the sensitivity, we estimate the expected discovery ( $\mathcal{Z}_{\text{dis}}$ ) and exclusion ( $\mathcal{Z}_{\text{exc}}$ ) limits by using the following formulae [131]:

$$\begin{aligned}\mathcal{Z}_{\text{dis}} &= \sqrt{2 \left[ (s+b) \ln \left( \frac{(s+b)(1+\delta_{\text{sys}}^2 b)}{b + \delta_{\text{sys}}^2 b(s+b)} \right) - \frac{1}{\delta_{\text{sys}}^2} \ln \left( 1 + \frac{\delta_{\text{sys}}^2 s}{1 + \delta_{\text{sys}}^2 b} \right) \right]}, \\ \mathcal{Z}_{\text{exc}} &= \sqrt{2 \left[ s - b \ln \left( \frac{b+s+x}{2b} \right) - \frac{1}{\delta_{\text{sys}}^2} \ln \left( \frac{b-s+x}{2b} \right) \right] - (b+s-x) \left( 1 + \frac{1}{\delta_{\text{sys}}^2 b} \right)},\end{aligned}\quad (4)$$

with

$$x = \sqrt{(s+b)^2 - 4\delta_{\text{sys}}^2 sb^2 / (1 + \delta_{\text{sys}}^2 b)}. \quad (5)$$

Here,  $s$  and  $b$  are the numbers of signal and background events, respectively, which can be obtained by multiplying the total signal and SM background cross sections, respectively, by the integrated luminosity while  $\delta$  is the percentage systematic error on the SM background estimate.

TABLE V: Cut flow of the cross sections (in fb) for the signals and SM backgrounds at  $\mu p - 1$  for the final state in Case 2. Here, we set a benchmark value of  $g^* = 0.1$ .

Cuts	Signals			Backgrounds			
	$T_{1500}$	$T_{2000}$	$T_{2500}$	$\nu tb$	$\nu W j$	$\nu Z j$	$\nu jj$
Basic	1.21	0.25	0.05	38160	11100	5365	378000
Cut 1	1.16	0.25	0.046	954	1576	268	17010
Cut 2	0.61	0.15	0.03	23	68	11	2438
Cut 3	0.39	0.094	0.018	2.67	0.33	0.53	2.04
Cut 4a	0.242	\	\	0.106	0.054	0.183	0.216
Cut 4b	\	0.078	0.017	0.021	0.054	0.125	0.087

TABLE VI: Cut flow of the cross sections (in fb) for the signals and SM backgrounds at  $\mu p - 2$  for the final state in Case 2. Here, we set a benchmark value of  $g^* = 0.1$ .

Cuts	Signals			Backgrounds			
	$T_{1500}$	$T_{2000}$	$T_{2500}$	$\nu tb$	$\nu W j$	$\nu Z j$	$\nu jj$
Basic	2.88	0.81	0.22	52920	14280	6980	480000
Cut 1	2.76	0.78	0.22	1534	2142	138	23520
Cut 2	1.44	0.46	0.13	45	114	58	377
Cut 3	0.86	0.29	0.084	4.76	0.61	0.77	0.53
Cut 4a	0.55	\	\	0.40	0.36	0.31	0.17
Cut 4b	\	0.24	0.08	0.167	0.248	0.24	0.082

In the limit case of  $\delta_{sys} \rightarrow 0$ , these expressions can be simplified to

$$\begin{aligned}\mathcal{Z}_{\text{dis}} &= \sqrt{2[(s+b)\ln(1+s/b) - s]}, \\ \mathcal{Z}_{\text{exc}} &= \sqrt{2[s - b\ln(1+s/b)]}.\end{aligned}\tag{6}$$

The integrated luminosity is set at  $100 \text{ fb}^{-1}$  for all three center-of-mass energies [96].

As a result, in Fig. 6, we present the 95% CL exclusion limit and  $5\sigma$  discovery reaches in the plane of  $g^* - m_T$  at the three different center-of-mass energies for Case 1. To illustrate the effect

TABLE VII: Cut flow of the cross sections (in fb) for the signals and SM backgrounds at  $\mu p - 3$  for the final state in Case 2. Here, we set a benchmark value of  $g^* = 0.1$ .

Cuts	Signals			Backgrounds			
	$T_{2000}$	$T_{3000}$	$T_{4000}$	$\nu tb$	$\nu W j$	$\nu Z j$	$\nu jj$
Basic	3.62	0.58	0.0884	89000	21480	10700	701400
Cut 1	3.54	0.58	0.088	3204	3651	2354	38577
Cut 2	2.32	0.4	0.062	196	301	107	982
Cut 3	1.22	0.232	0.036	12.5	1.85	1.07	2.1
Cut 4	1.09	0.226	0.035	0.56	0.47	0.39	0.22

of systematic uncertainty on the significance, we select three cases: no systematics ( $\delta = 0$ ) and two typical systematic uncertainties ( $\delta = 10\%$  and  $\delta = 20\%$ ). One can see that the higher systematic uncertainty of background can decrease the discovery capability and the exclusion power. With a realistic 10% systematic error, the discoverable (at  $5\sigma$  level) region is  $g^* \in [0.3, 0.5]$  with  $m_T \in [1500, 2100]$  GeV at  $\mu p - 1$ ,  $g^* \in [0.27, 0.5]$  with  $m_T \in [1500, 2400]$  GeV at  $\mu p - 2$ , and  $g^* \in [0.18, 0.5]$  with  $m_T \in [1500, 3250]$  GeV at  $\mu p - 3$ . As for the exclusion (at 95% CL) region, this is  $g^* \in [0.17, 0.5]$  with  $m_T \in [1500, 2500]$  GeV at  $\mu p - 1$ ,  $g^* \in [0.14, 0.5]$  with  $m_T \in [1500, 2900]$  GeV at  $\mu p - 2$ , and  $g^* \in [0.09, 0.5]$  with  $m_T \in [1500, 3700]$  GeV at  $\mu p - 3$ .

In Fig. 7, we present the 95% CL exclusion limit and  $5\sigma$  discovery reach in the plane of  $g^* - m_T$  at the three different center-of-mass energies for the fat jet final state (Case 2). One finds that the sensitivities are better than those for the signal in Case 1. In the presence of 10% systematic uncertainty, the discoverable (at  $5\sigma$  level) region is  $g^* \in [0.15, 0.5]$  with  $m_T \in [1500, 2520]$  GeV at  $\mu p - 1$ ,  $g^* \in [0.14, 0.5]$  with  $m_T \in [1500, 2900]$  GeV at  $\mu p - 2$ , and  $g^* \in [0.1, 0.5]$  with  $m_T \in [1800, 3750]$  GeV at  $\mu p - 3$ . As for the exclusion (at 95% CL) region, this is  $g^* \in [0.08, 0.5]$  with  $m_T \in [1500, 2850]$  GeV at  $\mu p - 1$ ,  $g^* \in [0.07, 0.5]$  with  $m_T \in [1500, 3340]$  GeV at  $\mu p - 2$ , and  $g^* \in [0.06, 0.5]$  with  $m_T \in [1800, 4500]$  GeV at  $\mu p - 3$ .

So far, we have treated the VLQ-T signals in Narrow Width Approximation (NWA), which is appropriate when the width-to-mass ratio  $\Gamma/M$  of the resonance is permille level, however, for values at percent level and beyond, the full Breit-Wigner (BW) should be adopted. In order to

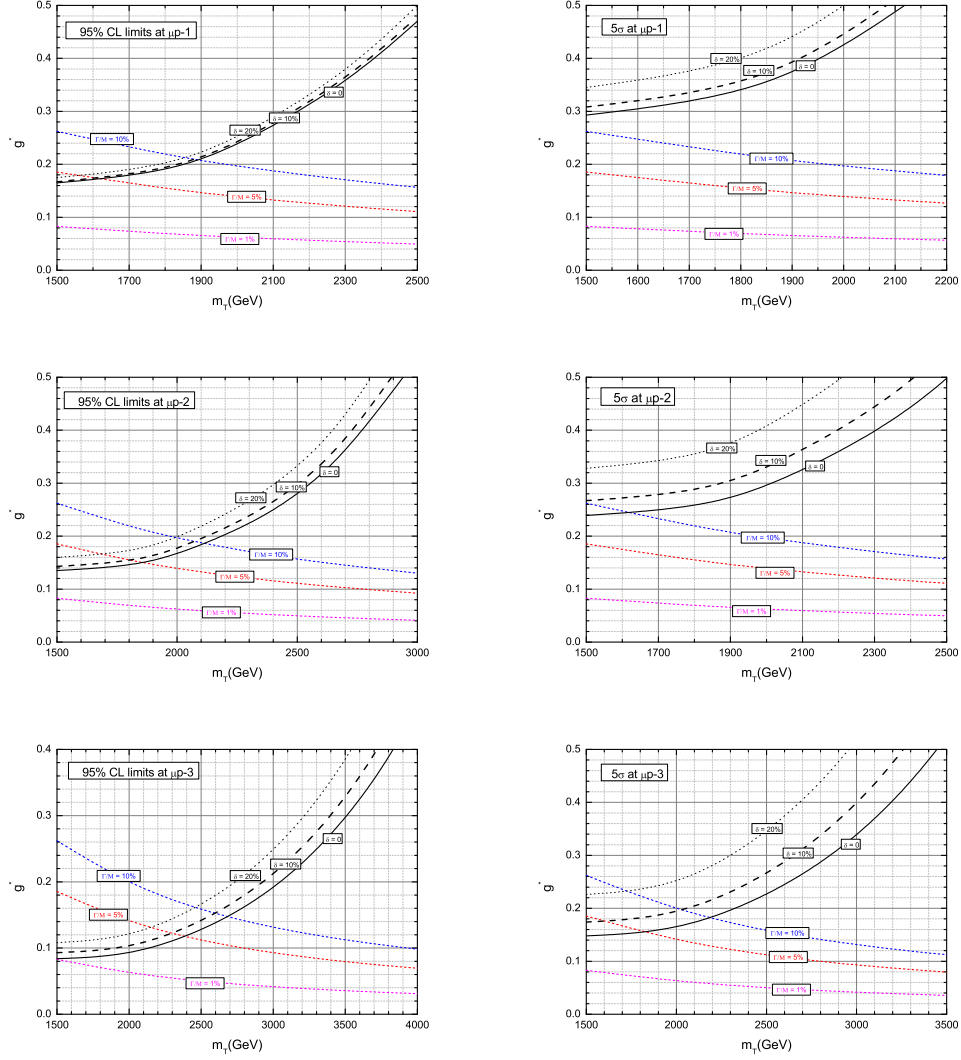


FIG. 6: 95% CL exclusion limit (left panel) and 5 $\sigma$  discovery reach (right panel) contour plots for the signal in  $g^* - m_T$  for Case 1 at  $\mu p\text{-}1$ ,  $\mu p\text{-}2$  and  $\mu p\text{-}3$ . Short-dashed lines denote the contours of  $\Gamma_T/m_T$ .

appreciate the difference between the two approaches in our case, we proceed as in Ref. [132] and limit ourselves to sample  $\Gamma_T/m_T$  values below 10%. Thus in Figs. 6 and 7, we also display the contours of  $\Gamma_T/m_T$  for three typical values: 1%, 5%, and 10%. For a fixed value of  $\Gamma_T/m_T = 10\%$  and systematic uncertainty of 10% within, e.g., Case 2 (the dominant final

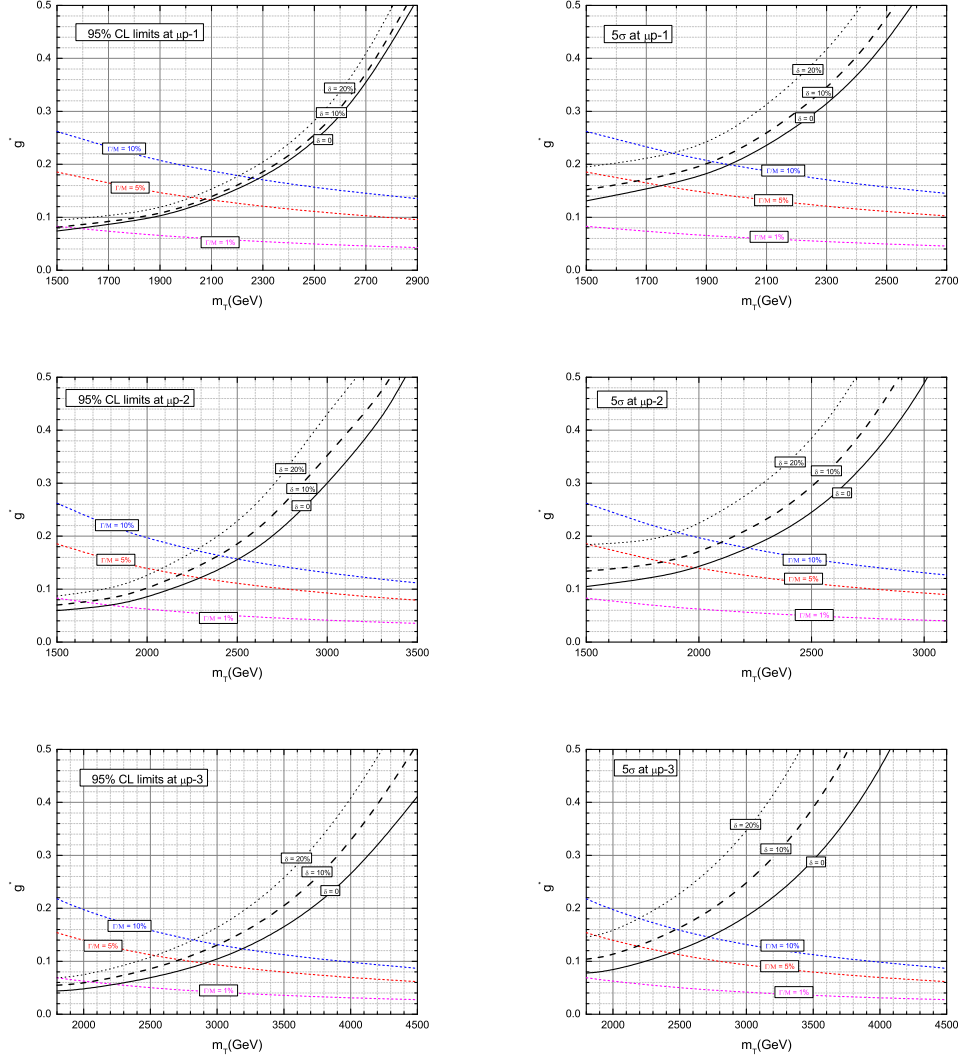


FIG. 7: 95% CL exclusion limit (left panel) and  $5\sigma$  discovery reach (right panel) contour plots for the signal in  $g^* - m_T$  for Case 2 at  $\mu p-1$ ,  $\mu p-2$  and  $\mu p-3$ . Short-dashed lines denote the contours of  $\Gamma_T/m_T$ .

state), the signal can be discovered (at  $5\sigma$  level) for a VLQ- $T$  mass of about 1900, 2000, and 2500 GeV at  $\mu p - 1$ ,  $\mu p - 2$ , and  $\mu p - 3$ , respectively. For the case of exclusion (at 95% CL), the lower limit on the VLQ- $T$  mass is about 2250, 2400, and 3000 GeV, at  $\mu p - 1$ ,  $\mu p - 2$ , and  $\mu p - 3$ , respectively. Hence, width effects can generally be significant.

Very recently, the authors of Ref. [121] have presented a comprehensive review of the most up-to-date exclusion limits on VLQs derived from ATLAS and CMS data at the LHC, wherein single VLQ- $T$  production constrains the mixing parameter  $\kappa$  to values below 0.26 (0.42) for  $m_T \sim 1.5$  (2.0) TeV. In Tab. VIII, we list some existing results related to searching for the singlet VLQ- $T$  at various of high-energy colliders. From this table, we expect that our study can drive complementary searches for a possible singlet VLQ- $T$  at a future muon-proton collider.

TABLE VIII: Some results of searching for the singlet VLQ- $T$  at different high-energy colliders. Here, the symbol “\” stands for no relevant results in the reference. The results in this work correspond to a mild systematic uncertainty of 10% at a  $\mu p$  collider with an integrated luminosity of  $100 \text{ fb}^{-1}$ .

Channel	Data Set	Excluding capability		Discovery capability		Reference
		$g^*$	$m_T/\text{TeV}$	$g^*$	$m_T/\text{TeV}$	
$T \rightarrow tZ$	LHC @14 TeV, $3 \text{ ab}^{-1}$	[0.06, 0.25]	[0.9, 1.5]	[0.10, 0.42]	[0.9, 1.5]	[133]
$T \rightarrow th$	LHC @14 TeV, $3 \text{ ab}^{-1}$	[0.16, 0.5]	[1.0, 1.6]	[0.24, 0.72]	[1.0, 1.6]	[134]
$T \rightarrow bW^+$	LHC @14 TeV, $3 \text{ ab}^{-1}$	[0.19, 0.5]	[1.3, 2.4]	[0.31, 0.5]	[1.3, 1.9]	[135]
$T \rightarrow bW^+$	$e\gamma$ collider @2 TeV, $1 \text{ ab}^{-1}$	[0.13, 0.5]	[0.8, 1.6]	\	\	[136]
$T \rightarrow tZ$	$e\gamma$ collider @3 TeV, $3 \text{ ab}^{-1}$	[0.15, 0.23]	[1.3, 2.0]	[0.23, 0.5]	[1.3, 2.0]	[137]
$T \rightarrow th$	$e\gamma$ collider @3 TeV, $3 \text{ ab}^{-1}$	[0.14, 0.50]	[1.3, 2.0]	[0.27, 0.5]	[1.3, 2.0]	[138]
$T \rightarrow bW^+$	$e^+e^-$ collider @3 TeV, $5 \text{ ab}^{-1}$	[0.15, 0.40]	[1.5, 2.6]	[0.24, 0.44]	[1.5, 2.4]	[139]
$T \rightarrow tZ$	$e^+e^-$ collider @3 TeV, $5 \text{ ab}^{-1}$	[0.19, 0.40]	[1.3, 2.5]	[0.31, 0.5]	[1.3, 2.3]	[140]
$T \rightarrow bW \rightarrow b\ell\nu$	$\mu p$ collider @4.58 TeV	[0.16, 0.48]	[1.5, 2.5]	[0.31, 0.5]	[1.5, 2.1]	this work
	$\mu p$ collider @6.48 TeV	[0.14, 0.5]	[1.5, 2.9]	[0.24, 0.5]	[1.5, 2.4]	
	$\mu p$ collider @9.16 TeV	[0.09, 0.4]	[1.5, 3.7]	[0.18, 0.5]	[1.5, 3.2]	
$T \rightarrow bW \rightarrow bJ$	$\mu p$ collider @4.58 TeV	[0.08, 0.5]	[1.5, 2.85]	[0.14, 0.5]	[1.5, 2.52]	
	$\mu p$ collider @6.48 TeV	[0.07, 0.5]	[1.5, 3.34]	[0.13, 0.5]	[1.5, 2.9]	
	$\mu p$ collider @9.16 TeV	[0.06, 0.5]	[2.0, 4.5]	[0.1, 0.5]	[1.8, 3.75]	

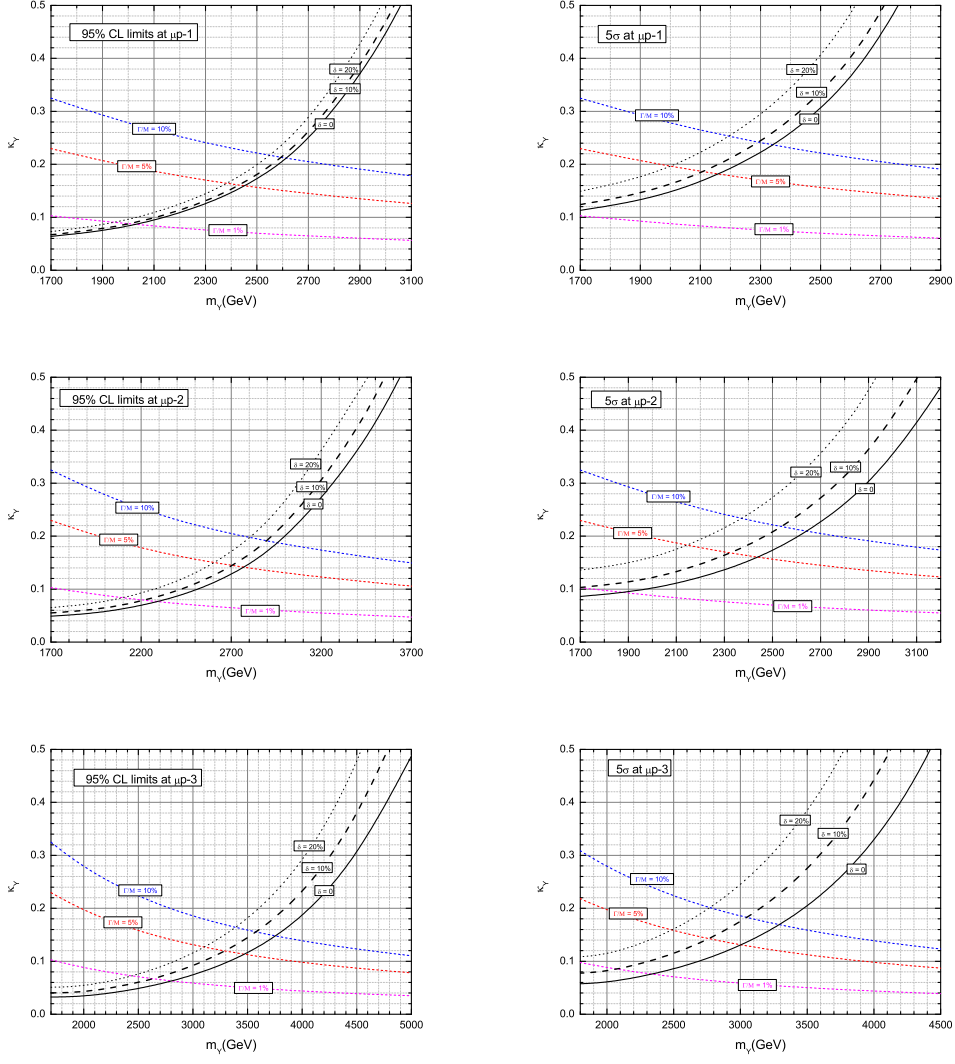


FIG. 8: 95% CL exclusion limit (left panel) and 5 $\sigma$  discovery reach (right panel) contour plots for the signal in  $\kappa - m_Y$  for Case 2 at  $\mu p-1$ ,  $\mu p-2$  and  $\mu p-3$ . Short-dashed lines denote the contours of  $\Gamma_Y/m_Y$ .

## B. Expected discovery and exclusion reaches for VLQ-Y

As explained, the MC analysis for the VLQ-Y case is identical to the previous one. Thus, similarly to what previously done, in Fig. 8, we present the 95% CL exclusion limit and 5 $\sigma$

discovery reach in the plane of  $\kappa_Y - m_Y$  at the usual three different center-of-mass energies, albeit limitedly to the fat jet final state (the dominant one, thereby neglecting the subdominant leptonic signal). In the presence of 10% systematic uncertainty, the discoverable (at  $5\sigma$  level) region is  $\kappa_Y \in [0.12, 0.5]$  with  $m_Y \in [1700, 2700]$  GeV at  $\mu p - 1$ ,  $\kappa_Y \in [0.10, 0.5]$  with  $m_Y \in [1700, 3100]$  GeV at  $\mu p - 2$ , and  $\kappa_Y \in [0.08, 0.5]$  with  $m_Y \in [1700, 4100]$  GeV at  $\mu p - 3$ . Instead, a VLQ- $Y$  can be excluded (at 95% CL) for  $\kappa_Y \in [0.07, 0.5]$  with  $m_Y \in [1700, 3020]$  GeV at  $\mu p - 1$ ,  $\kappa_Y \in [0.06, 0.5]$  with  $m_Y \in [1700, 3540]$  GeV at  $\mu p - 2$ , and  $\kappa_Y \in [0.04, 0.5]$  with  $m_Y \in [1700, 4800]$  GeV at  $\mu p - 3$ . Furthermore, for a fixed value of  $\Gamma_Y/m_Y = 10\%$ , the VLQ- $Y$  can be discovered (at  $5\sigma$  level) with a mass of about 2300, 2500, and 3000 GeV at  $\mu p - 1$ ,  $\mu p - 2$ , and  $\mu p - 3$ , respectively. Instead, the 95% CL excluded region for the VLQ- $T$  mass is below about 2600, 2900, and 3600 GeV at  $\mu p - 1$ ,  $\mu p - 2$  and  $\mu p - 3$ , respectively.

Very recently, the authors of Ref. [63] investigated the expected limits for the VLQ- $Y$  state via single production of  $Y$  followed by decay channel  $Y \rightarrow Wb$  at the LHC with  $\sqrt{s} = 14$  TeV and the future high-energy  $pp$  colliders. Considering an integrated luminosity of 300 (3000)  $\text{fb}^{-1}$  at the 14 TeV LHC with a systematic uncertainty  $\delta = 10\%$ , the VLQ- $Y$  can be discovered (at  $5\sigma$  level) over the region  $\kappa_Y \in [0.11, 0.5]$  with  $m_Y \in [1500, 3200]$  GeV ( $\kappa_Y \in [0.1, 0.5]$  with  $m_Y \in [1500, 3350]$  GeV), and excluded (at 95% CL) over the region  $\kappa_Y \in [0.06, 0.5]$  with  $m_Y \in [1500, 3800]$  GeV ( $\kappa_Y \in [0.05, 0.5]$  with  $m_Y \in [1500, 3970]$  GeV). For a fixed value of  $\Gamma_Y/m_Y = 10\%$ , the VLQ- $Y$  can be discovered (excluded) with a mass about 2200 (2600) GeV at the High-Luminosity LHC (HL-LHC). Besides, the authors of Ref. [64] studied single production of VLQ- $Y$  at the HL-LHC with  $\sqrt{s} = 14$  TeV via the fully hadronic mode  $Y \rightarrow bW \rightarrow bjj$ . For the integrated luminosity projection of 3000  $\text{fb}^{-1}$  and  $\kappa_Y = 0.5$  (0.3), the lower limits for  $m_Y$  were obtained as 2350 (1550) GeV for exclusion (at 95% CL), and 1900 (1250) GeV for discovery (at  $5\sigma$  level). Thus, we conclude again that our study can drive complementary searches for a possible doublet VLQ- $Y$  at a future muon-proton collider.

#### IV. CONCLUSIONS

In this paper, we have studied the potential of a future  $\mu p$  collider to search for heavy VLQs of type  $T$  and  $Y$  via the single production mode  $\mu g \rightarrow \nu_\mu bT/Y$  and subsequent decay  $T/Y \rightarrow bW$ . To be as model-independent as possible, a simplified framework with only

two free parameters was applied: the VLQs mass  $m_{T/Y}$  and the EW coupling constant  $g^*/\kappa_Y$ . Specifically, we have presented a search strategy at such a possible future machine with the three typical center-of-mass energies  $\sqrt{s} = 5.29$  (labelled  $\mu p - 1$ ), 6.48 (labelled  $\mu p - 2$ ), and 9.16 (labelled  $\mu p - 3$ ) TeV, for VLQ- $T$  and VLQ- $Y$  signals with two final states: one electrons plus one  $b$ -tagged jet and missing energy (Case 1) and one fat jet plus one  $b$ -tagged jet (Case 2). After performing a detector level simulation for the signal and relevant SM backgrounds, the  $5\sigma$  discovery prospects and 95% CL exclusion limits over the relevant parameter space were obtained.

From the numerical results, all tested against existing experimental results from the LHC from searches for VLQ, we have obtained the following results.

1. Due to a larger cross section for the final state including a fat  $W$ -jet with respect to the leptonic  $W$  decay channel, the sensitivities in Case 2 are better than those in Case 1, respectively.
2. Considering a systematic uncertainty of 10% with an integrated luminosity of  $100 \text{ fb}^{-1}$ , for the VLQ- $T$ , the discoverable (at  $5\sigma$  level) region is  $g^* \in [0.15, 0.5]$  with  $m_T \in [1500, 2520] \text{ GeV}$  at  $\mu p - 1$ , gradually changing to  $g^* \in [0.13, 0.5]$  with  $m_T \in [1500, 2900] \text{ GeV}$  at  $\mu p - 2$ , and to  $g^* \in [0.1, 0.5]$  with  $m_T \in [1800, 3750] \text{ GeV}$  at  $\mu p - 3$ . Conversely, the 95% CL exclusion limit is attained over the parameter space region  $g^* \in [0.08, 0.5]$  with  $m_T \in [1500, 2750] \text{ GeV}$  at  $\mu p - 1$ ,  $g^* \in [0.07, 0.5]$  with  $m_T \in [1500, 3340] \text{ GeV}$  at  $\mu p - 2$ , and  $g^* \in [0.06, 0.5]$  with  $m_T \in [1800, 4500] \text{ GeV}$  at  $\mu p - 3$ .
3. For the above systematic uncertainty and integrated luminosity, in the case of the VLQ- $Y$ , the discoverable (at  $5\sigma$  level) region is  $\kappa_Y \in [0.12, 0.5]$  with  $m_Y \in [1700, 2700] \text{ GeV}$  at  $\mu p - 1$ ,  $\kappa_Y \in [0.10, 0.5]$  with  $m_Y \in [1700, 3100] \text{ GeV}$  at  $\mu p - 2$ , and  $\kappa_Y \in [0.08, 0.5]$  with  $m_Y \in [1700, 4100] \text{ GeV}$  at  $\mu p - 3$ . Conversely, the 95% CL exclusion limit is attained over the parameter space of  $\kappa_Y \in [0.07, 0.5]$  with  $m_Y \in [1700, 3020] \text{ GeV}$  at  $\mu p - 1$ ,  $\kappa_Y \in [0.06, 0.5]$  with  $m_Y \in [1700, 3540] \text{ GeV}$  at  $\mu p - 2$ , and  $\kappa_Y \in [0.04, 0.5]$  with  $m_Y \in [1700, 4800] \text{ GeV}$  at  $\mu p - 3$ .
4. As previous literature has emphasised the role of the  $T$  and  $Y$  width in the case of their single production mode at the LHC, for a fixed value of  $\Gamma_{T/Y}/m_{T/Y} = 10\%$ , the VLQ-

$T$  ( $Y$ ) can be discovered (at  $5\sigma$  level) with a mass about 1900 (2300), 2000 (2500), and 2500 (3000) GeV at  $\mu p = 1$ ,  $\mu p = 2$ , and  $\mu p = 3$ , respectively. Conversely, the 95% CL exclusion limit is attained for VLQ- $T$  mass about 2250 (2600), 2400 (2900), and 3000 (3600) GeV, at  $\mu p = 1$ , the  $\mu p = 2$  and the  $\mu p = 3$ , respectively.

Finally, by comparing our results to existing literature on the VLQ- $T$  and VLQ- $Y$  states at a variety of present and future colliders, we have concluded that a future  $\mu p$  machine can be competitive in the search for such possible new states of Nature.

### Acknowledgments

The work of J-ZH and Y-BL is supported by the Natural Science Foundation of Henan Province (Grant No. 242300421398). The work of SM is supported in part through the NExT Institute and the STFC Consolidated Grant ST/X000583/1. L000296/1.

---

- [1] N. Arkani-Hamed, A. G. Cohen, E. Katz, A. E. Nelson, T. Gregoire and J. G. Wacker, *JHEP* **08**, 021 (2002).
- [2] N. Arkani-Hamed, A. G. Cohen, E. Katz, and A. E. Nelson, *JHEP* **07**, 034 (2002).
- [3] T. Han, H. E. Logan, B. McElrath and L. T. Wang, *Phys. Rev. D* **67**, 095004 (2003).
- [4] S. Chang and H. J. He, *Phys. Lett. B* **586**, 95-105 (2004).
- [5] K. Agashe, R. Contino, and A. Pomarol, *Nucl. Phys. B* **719** 165 (2005).
- [6] R. Contino, L. Da Rold and A. Pomarol, *Phys. Rev. D* **75**, 055014 (2007).
- [7] P. Lodone, *JHEP* **12**, 029 (2008).
- [8] O. Matsedonskyi, G. Panico and A. Wulzer, *JHEP* **01**, 164 (2013).
- [9] R. Benbrik, M. Boukidi and S. Moretti, *Phys. Rev. D* **109**, no.5, 055016 (2024).
- [10] A. Arhrib, R. Benbrik, M. Boukidi, B. Manaut and S. Moretti, [arXiv:2401.16219](https://arxiv.org/abs/2401.16219) [hep-ph].
- [11] A. Arhrib, R. Benbrik, M. Boukidi and S. Moretti, *Eur. Phys. J. C* **84**, no.10, 1008 (2024).
- [12] A. Arhrib, R. Benbrik, M. Berrouj, M. Boukidi and B. Manaut, [arXiv:2407.01348](https://arxiv.org/abs/2407.01348) [hep-ph].
- [13] R. Benbrik, M. Berrouj and M. Boukidi, [arXiv:2408.15985](https://arxiv.org/abs/2408.15985) [hep-ph].
- [14] A. Arhrib, R. Benbrik, M. Boukidi and S. Moretti, [arXiv:2409.20104](https://arxiv.org/abs/2409.20104) [hep-ph].
- [15] H. J. He, T. M. P. Tait and C. P. Yuan, *Phys. Rev. D* **62**, 011702(R) (2000).

- [16] X. F. Wang, C. Du and H. J. He, *Phys. Lett. B* **723**, 314-323 (2013).
- [17] H. J. He, C. T. Hill and T. M. P. Tait, *Phys. Rev. D* **65**, 055006 (2002).
- [18] H. J. He and Z. Z. Xianyu, *JCAP* **10**, 019 (2014).
- [19] J. A. Aguilar-Saavedra, R. Benbrik, S. Heinemeyer, and M. Pérez-Victoria,, *Phys. Rev. D* **88**, 094010 (2013).
- [20] H. J. He, N. Polonsky and S. f. Su, *Phys. Rev. D* **64**, 053004 (2001).
- [21] N. Chen and H. J. He, *JHEP* **04**, 062 (2012).
- [22] M. L. Xiao and J. H. Yu, *Phys. Rev. D* **90**, no.1, 014007 (2014).
- [23] K. Y. Cingiloglu and M. Frank, *Phys. Rev. D* **109**, no.3, 036016 (2024).
- [24] K. Cheung, W. Y. Keung, C. T. Lu and P. Y. Tseng, *JHEP* **05**, 117 (2020).
- [25] A. Crivellin, M. Kirk, T. Kitahara and F. Mescia, *JHEP* **03**, 234 (2023).
- [26] B. Belfatto and Z. Berezhiani, *JHEP* **10**, 079 (2021).
- [27] G. C. Branco, J. T. Penedo, P. M. F. Pereira, M. N. Rebelo and J. I. Silva-Marcos, *JHEP* **07**, 099 (2021)
- [28] F. J. Botella, G. C. Branco, M. N. Rebelo, J. I. Silva-Marcos and J. F. Bastos, *Eur. Phys. J. C* **82**, no.4, 360 (2022) [erratum: *Eur. Phys. J. C* **82**, 423 (2022)].
- [29] J. Cao, L. Meng, L. Shang, S. Wang and B. Yang, *Phys. Rev. D* **106**, no.5, 055042 (2022).
- [30] A. Crivellin, M. Kirk, T. Kitahara and F. Mescia, *Phys. Rev. D* **106**, no.3, L031704 (2022).
- [31] S. P. He, *Chin. Phys. C* **47**, no.4, 043102 (2023).
- [32] G. C. Branco and M. N. Rebelo, [arXiv:2208.07235](https://arxiv.org/abs/2208.07235) [hep-ph].
- [33] H. Abouabid, A. Arhrib, R. Benbrik, M. Boukidi and J. E. Falaki, *J. Phys. G* **51**, no.7, 075001 (2024).
- [34] A. De Simone, O. Matsedonskyi, R. Rattazzi and A. Wulzer, *JHEP* **04**, 004 (2013).
- [35] M. Buchkremer, G. Cacciapaglia, A. Deandrea, and L. Panizzi, *Nucl. Phys. B* **876**, 376-417 (2013).
- [36] J. A. Aguilar-Saavedra, *JHEP* **11**, 030 (2009).
- [37] J. Mrazek and A. Wulzer, *Phys. Rev. D* **81**, 075006 (2010).
- [38] G. Dissertori, E. Furlan, F. Moortgat and P. Nef, *JHEP* **09**, 019 (2010).
- [39] A. Atre, G. Azuelos, M. Carena, T. Han, E. Ozcan, J. Santiago and G. Unel, *JHEP* **08**, 080 (2011).
- [40] G. Cacciapaglia, A. Deandrea, L. Panizzi, N. Gaur, D. Harada and Y. Okada,

JHEP **03**, 070 (2012).

- [41] G. Cacciapaglia, A. Deandrea, L. Panizzi, S. Perries and V. Sordini, JHEP **03**, 004 (2013).
- [42] S. Gopalakrishna, T. Mandal, S. Mitra and G. Moreau, JHEP **08**, 079 (2014).
- [43] O. Matsedonskyi, G. Panico and A. Wulzer, JHEP **12**, 097 (2014).
- [44] M. Backović, T. Flacke, S. J. Lee and G. Perez, JHEP **09**, 022 (2015).
- [45] C. H. Chen and T. Nomura, Phys. Rev. D **94**, no.3, 035001 (2016).
- [46] B. Fuks and H. S. Shao, Eur. Phys. J. C **77**, no.2, 135 (2017).
- [47] Y. B. Liu, Phys. Rev. D **95**, no.3, 035013 (2017).
- [48] J. A. Aguilar-Saavedra, D. E. López-Fogliani and C. Muñoz, JHEP **06**, 095 (2017).
- [49] X. M. Cui, Y. Q. Li and Y. B. Liu, Phys. Rev. D **106**, no.11, 115025 (2022).
- [50] K. P. Xie, G. Cacciapaglia and T. Flacke, JHEP **10**, 134 (2019).
- [51] R. Benbrik, E. B. Kuutmann, D. Buarque Franzosi, V. Ellajosyula, R. Enberg, G. Ferretti, M. Isackson, Y. B. Liu, T. Mandal, T. Mathisen, *et al.* JHEP **05**, 028 (2020).
- [52] J. A. Aguilar-Saavedra, J. Alonso-González, L. Merlo and J. M. No, Phys. Rev. D **101**, no.3, 035015 (2020).
- [53] A. Belyaev, R. S. Chivukula, B. Fuks, E. H. Simmons and X. Wang, Phys. Rev. D **104**, no.9, 095024 (2021).
- [54] A. Bhardwaj, T. Mandal, S. Mitra and C. Neeraj, Phys. Rev. D **106**, no.9, 095014 (2022).
- [55] A. Bhardwaj, K. Bhide, T. Mandal, S. Mitra and C. Neeraj, Phys. Rev. D **106**, no.7, 075024 (2022).
- [56] S. Verma, S. Biswas, A. Chatterjee and J. Ganguly, Phys. Rev. D **107**, no.11, 115024 (2023).
- [57] J. Bardhan, T. Mandal, S. Mitra and C. Neeraj, Phys. Rev. D **107**, no.11, 115001 (2023).
- [58] J. M. Alves, G. C. Branco, A. L. Cherchiglia, C. C. Nishi, J. T. Penedo, P. M. F. Pereira, M. N. Rebelo and J. I. Silva-Marcos, Phys. Rept. **1057**, 1-69 (2024).
- [59] A. C. Canbay and O. Cakir, Phys. Rev. D **108**, no.9, 095006 (2023).
- [60] A. Belyaev, R. S. Chivukula, B. Fuks, E. H. Simmons and X. Wang, Phys. Rev. D **108**, no.3, 3 (2023).
- [61] L. Han, S. Wang, L. Shang and B. Yang, Chin. Phys. C **47**, no.4, 043108 (2023).
- [62] Y. B. Liu, B. Hu and C. Z. Li, Nucl. Phys. B **1007**, 116667 (2024).
- [63] L. Shang, Y. Yan, S. Moretti and B. Yang, Phys. Rev. D **109**, no.11, 115016 (2024).

- [64] V. Cetinkaya, A. Ozansoy, V. Ari, O. M. Ozsimsek and O. Cakir, *Nucl. Phys. B* **973**, 115580 (2021).
- [65] Y. J. Zhang, J. L. Chang and T. G. Liu, *Chin. Phys. C* **48**, no.7, 073104 (2024).
- [66] B. Yang, Z. Li, X. Jia, S. Moretti and L. Shang, *Eur. Phys. J. C* **84**, no.10, 1124 (2024).
- [67] G. Aad *et al.* [ATLAS], *Phys. Lett. B* **854**, 138743 (2024).
- [68] G. Aad *et al.* [ATLAS], *Phys. Lett. B* **843**, 138019 (2023).
- [69] A. Tumasyan *et al.* [CMS], *JHEP* **07**, 020 (2023).
- [70] M. Aaboud *et al.* (ATLAS Collaboration), *Phys. Rev. D* **98**, 092005 (2018).
- [71] M. Aaboud *et al.* (ATLAS Collaboration), *JHEP* **12**, 039 (2018).
- [72] M. Aaboud *et al.* (ATLAS Collaboration), *JHEP* **08**, 048 (2018).
- [73] M. Aaboud *et al.* (ATLAS Collaboration), *JHEP* **05**, 164 (2019).
- [74] A. M. Sirunyan *et al.* (CMS Collaboration), *Eur. Phys. J. C* **79**, 364 (2019).
- [75] A. M. Sirunyan *et al.* (CMS Collaboration), *JHEP* **08**, 177 (2018).
- [76] M. Aaboud *et al.* (ATLAS Collaboration), *Phys. Rev. Lett.* **121**, 211801 (2018).
- [77] A. M. Sirunyan *et al.* (CMS Collaboration), *Phys. Rev. D* **100**, 072001 (2019).
- [78] A. Buckley, J. M. Butterworth, L. Corpe, D. Huang, and P. Sun, *SciPost Phys.* **9**, 069 (2020).
- [79] S. Moretti, D. O'Brien, L. Panizzi, and H. Prager, *Phys. Rev. D* **96**, 075035 (2017).
- [80] A. Carvalho, S. Moretti, D. O'Brien, L. Panizzi, and H. Prager, *Phys. Rev. D* **98**, 015029 (2018).
- [81] A. Deandrea, T. Flacke, B. Fuks, L. Panizzi, and H. S. Shao, *JHEP* **08**, 107 (2021).
- [82] G. Aad *et al.* [ATLAS], *Phys. Rev. D* **105**, no.9, 092012 (2022).
- [83] G. Aad *et al.* [ATLAS], *JHEP* **08**, 153 (2023).
- [84] G. Aad *et al.* [ATLAS], *Phys. Rev. D* **109**, no.11, 112012 (2024).
- [85] G. Aad *et al.* [ATLAS], arXiv:2408.08789 [hep-ex].
- [86] G. Aad *et al.* [ATLAS], arXiv:2409.20273 [hep-ex].
- [87] A. Tumasyan *et al.* [CMS], *JHEP* **09**, 057 (2023).
- [88] A. Hayrapetyan *et al.* [CMS], *Phys. Rev. D* **110**, no.7, 072012 (2024).
- [89] A. Hayrapetyan *et al.* [CMS], arXiv:2405.17605 [hep-ex].
- [90] V. D. Shiltsev, Conf. Proc. C **970512**, 420-421 (1997) FERMILAB-CONF-97-114.
- [91] I. F. Ginzburg, Turk. J. Phys. **22**, 607-610 (1998).
- [92] K. Cheung, *AIP Conf. Proc.* **441**, no.1, 338-344 (1998).

- [93] K. Cheung, *AIP Conf. Proc.* **542**, no.1, 160-170 (2000).
- [94] M. Carena, D. Choudhury, C. Quigg and S. Raychaudhuri, *Phys. Rev. D* **62**, 095010 (2000).
- [95] U. Kaya, B. Ketenoglu and S. Sultansoy, [arXiv:1807.09867](#) [physics.acc-ph].
- [96] U. Kaya, B. Ketenoglu, S. Sultansoy and F. Zimmermann, [arXiv:1905.05564](#) [physics.acc-ph].
- [97] B. Ketenoglu, B. Dağlı, A. Öztürk and S. Sultansoy, *Mod. Phys. Lett. A* **37**, no.37n38, 2230013 (2022).
- [98] B. Dagli, B. Ketenoglu and S. Sultansoy, [arXiv:2206.00037](#) [physics.acc-ph].
- [99] U. Kaya, B. Ketenoglu, S. Sultansoy and F. Zimmermann, *EPL* **138**, no.2, 24002 (2022).
- [100] D. Akturk, B. Dagli, B. Ketenoglu, A. Ozturk and S. Sultansoy, [arXiv:2406.02647](#) [hep-ph].
- [101] A. Caliskan, S. O. Kara and A. Ozansoy, *Adv. High Energy Phys.* **2017**, 1540243 (2017).
- [102] Y. C. Acar, U. Kaya and B. B. Oner, *Chin. Phys. C* **42**, no.8, 083108 (2018)
- [103] A. Caliskan, [arXiv:1802.09874](#) [hep-ph].
- [104] E. Alici and M. Köksal, *Mod. Phys. Lett. A* **34**, no.36, 1950298 (2019).
- [105] A. Ozansoy, *Communications Faculty of Sciences University of Ankara Series A2-A3: Physical Sciences and Engineering* **2020**, 1-10.
- [106] S. Spor, A. A. Billur and M. Köksal, *Eur. Phys. J. Plus* **135**, no.8, 683 (2020).
- [107] K. Cheung and Z. S. Wang, *Phys. Rev. D* **103**, 116009 (2021).
- [108] G. Aydin, Y. O. Günaydin, M. T. Tarakcioglu, M. Sahin and S. Sultansoy, *Acta Phys. Polon. B* **53**, no.11, 3 (2022).
- [109] E. Gurkanli, [arXiv:2403.10263](#) [hep-ph].
- [110] E. Alici, [arXiv:2410.19329](#) [hep-ph].
- [111] Y. B. Liu, *Nucl. Phys. B* **923**, 312-323 (2017).
- [112] L. Han, Y. J. Zhang and Y. B. Liu, *Phys. Lett. B* **771**, 106-112 (2017).
- [113] Y. J. Zhang, L. Han and Y. B. Liu, *Phys. Lett. B* **768**, 241-247 (2017).
- [114] X. Gong, C. X. Yue, H. M. Yu and D. Li, *Eur. Phys. J. C* **80**, no.9, 876 (2020)
- [115] L. Shang, C. Chen, S. Wang and B. Yang, *Nucl. Phys. B* **984**, 115977 (2022).
- [116] H. J. He, Y. P. Kuang, and X. y. Li, *Phys. Rev. Lett.* **69**, 2619 (1992).
- [117] H. J. He, Y. P. Kuang, and X. y. Li, *Phys. Rev. D* **49**, 4842 (1994).
- [118] H. J. He, Y. P. Kuang, and C. P. Yuan, *Phys. Rev. D* **51**, 6463 (1995).
- [119] H. J. He, Y. P. Kuang, and C. P. Yuan, *Phys. Rev. D* **55**, 3038 (1997).
- [120] H. J. He and W. B. Kilgore, *Phys. Rev. D* **55**, 1515 (1997).

- [121] R. Benbrik, M. Boukidi, M. Ech-chaouy, S. Moretti, K. Salime and Q. S. Yan, arXiv:2412.01761 [hep-ph].
- [122] J. Alwall, R. Frederix, S. Frixione, V. Hirschi, F. Maltoni, O. Mattelaer, H.-S. Shao, T. Stelzer, P. Torrielli, and M. Zaro, **JHEP** **07**, 079 (2014).
- [123] R. D. Ball *et al.* [NNPDF Collaboration], **JHEP** **04**, 040 (2015).
- [124] T. Sjöstrand, S. Ask, J. R. Christiansen *et al.*, **Comput. Phys. Commun.** **191**, 159 (2015).
- [125] J. de Favereau *et al.* (DELPHES 3 Collaboration), **JHEP** **02**, 057 (2014).
- [126] Y. L. Dokshitzer, G. D. Leder, S. Moretti and B. R. Webber, **JHEP** **08**, 001 (1997).
- [127] M. Wobisch and T. Wengler, arXiv:hep-ph/9907280 [hep-ph].
- [128] M. Cacciari, G. P. Salam and G. Soyez, **Eur. Phys. J. C** **72**, 1896 (2012).
- [129] E. Conte, B. Fuks, and G. Serret, **Comput. Phys. Commun.** **184**, 222 (2013).
- [130] E. Conte, B. Dumont, B. Fuks and C. Wymant, **Eur. Phys. J. C** **74**, no. 10, 3103 (2014).
- [131] G. Cowan, K. Cranmer, E. Gross, and O. Vitells, **Eur. Phys. J. C** **71**, 1554 (2011) [erratum: **Eur. Phys. J. C** **73**, 2501 (2013)].
- [132] D. Barducci, A. Belyaev, J. Blamey, S. Moretti, L. Panizzi and H. Prager, **JHEP** **07**, 142 (2014).
- [133] Y. B. Liu and Y. Q. Li, **Eur. Phys. J. C** **77**, 654 (2017).
- [134] Y. B. Liu and S. Moretti, **Phys. Rev. D** **100**, 015025 (2019).
- [135] B. Yang, M. Wang, H. Bi and L. Shang, **Phys. Rev. D** **103**, no.3, 036006 (2021).
- [136] B. Yang, H. Shao, and J. Han, **Eur. Phys. J. C** **78**, 184 (2018).
- [137] L. Shang, D. Zhang, and B. Yang, **Phys. Rev. D** **100**, 075032 (2019).
- [138] L. Shang, W. Wei, and B. Yang, **Nucl. Phys.** **B955**, 115058 (2020).
- [139] X. Qin, L. F. Du, and J. F. Shen, **Nucl. Phys.** **B979**, 115784 (2022).
- [140] L. Han, L. F. Du and Y. B. Liu, **Phys. Rev. D** **105**, no.11, 115032 (2022).